Algae Pyrolysis in Molten NaOH–Na 2 CO 3 for Hydrogen Production

Jun Li, Kuo Zeng, Dian Zhong, Gilles Flamant, Ange Nzihou, Claire White, Haiping Yang, Hanping Chen

Algae Pyrolysis in Molten NaOH−Na_2CO_3 for Hydrogen Production

Jun Li, Kuo Zeng,* Dian Zhong, Gilles Flamant, Ange Nzihou, Claire E. White, Haiping Yang, and Hanping Chen

ABSTRACT: Biomass pyrolysis within the alkaline molten salt is attractive due to its ability to achieve high hydrogen yield under relatively mild conditions. However, poor contact between biomass, especially the biomass pellet, and hydroxide during the slow heating process, as well as low reaction temperatures, become key factors limiting the hydrogen production. To address these challenges, fast pyrolysis of the algae pellet in molten NaOH−Na_2CO_3 was conducted at 550, 650, and 750 °C. Algae were chosen as feedstock for their high photosynthetic efficiency and growth rate, and the concept of coupling molten salt with concentrated solar energy was proposed to address the issue of high energy consumption at high temperatures. At 750 °C, the pollutant gases containing Cl and S were completely removed, and the HCN removal rate reached 44.92%. During the continuous pyrolysis process, after a slight increase, the hydrogen yield remained stable at 71.48 mmol/g-algae and constituted 86.10% of the gas products, and a minimum theoretical hydrogen production efficiency of algae can reach 84.86%. Most importantly, the evolution of physicochemical properties of molten NaOH−Na_2CO_3 was revealed for the first time. Combined with the conversion characteristics of feedstock and gas products, this study provides practical guidance for large-scale application of molten salt including feedstock, operation parameters, and post-treatment process.

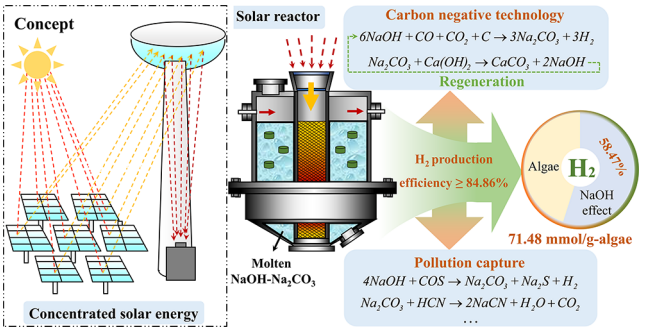

1. INTRODUCTION

Hydrogen is considered as an ideal future energy vector due to its high energy density associated with no pollutants and greenhouse gases production, which can significantly alleviate the energy crisis and global warming caused by the consumption of fossil fuels.[1] Most technologies for hydrogen production rely on fossil energy, among them are coal/petroleum gasification and steam methane reforming, which are responsible for about 95% of the global hydrogen production.[2] Nevertheless, hydrogen production can only be environmentally friendly if the feedstock resource used to produce hydrogen is biomass rather than fossil fuels and the energy resource is a renewable source such as solar thermal or wind energy.[3] As a third-generation biomass resource, algae have excellent advantages such as high photosynthetic efficiency, fast growth rate, high CO_2 fixation capacity, and no need for arable land.[4] As a result, many researchers have developed ways for hydrogen production from algae.

Thermal−chemical and bio-chemical methods are two main ways to produce algae-based hydrogen, of which thermal−chemical methods such as pyrolysis, gasification, and super/subcritical hydrothermal treatment are favored due to their high reaction rate.[5] Unfortunately, these technologies often suffer from high energy consumption, high operation pressure, salt precipitation (ash in algae), low hydrogen yield, and so forth.[6−8] Thus, there is a need for an economical and efficient method to convert algae into high-yield hydrogen in an environmentally friendly manner. Saxena first proposed alkaline thermal treatment (ATT) in 2003,[9] which employed sodium hydroxide to act as a hydrogen donor for hydrogen production while facilitating the fragmentation of biomass (which is not available with alkaline carbonates), as shown in reaction 1. Compared with conventional thermal−chemical methods, ATT can be operated at atmospheric pressure and lower temperatures (<500 °C), allowing a more efficient conversion of biomass to hydrogen and absence of carbon monoxide and carbon dioxide formation, while still maintaining a certain amount of ash.[10−13] Hydroxides has the ability to destroy the original structure of the biomass[5] and serve as a hydrogen donor for hydrogen production. Besides, the evolution of physicochemical properties of alkaline molten

salt during thermochemical processes has also been little studied

$$2NaOH_{(s)} + C_{(s)} + H_2O_{(g)} \rightarrow 2H_{2(g)} + Na_2CO_{3(s)} \quad (1)$$

In recent years, researchers have conducted a series of in-depth parametric studies on ATT, including feedstock types,[14] reaction conditions,[15] hydroxide types,[11] and in situ/ex situ catalyst types,[12,16,17] in order to determine an optimal route for hydrogen production by AAT. In addition, kinetic/mechanistic investigations were performed.[10] However, these studies resulted in limited performance due to the complicated process caused by multi-stage catalysis or insufficient hydrogen production efficiency due to the low heating rate. Taking the ATT process of seaweed as an example,[14] when the reaction temperature rises to the melting point of NaOH (319 °C), the seaweed floats on the surface of molten NaOH due to the difference in density, and the contact area of the feedstock with NaOH is significantly reduced. In addition, the devolatilization temperature range of algae is higher than the melting point of NaOH (as is the case for the majority of biomass),[18,19] consequently, most of the biomass/volatiles are converted without reacting with NaOH. This weakness is strengthened when the feedstock is fed in pellets. In fact, pelleting of biomass is an efficient solution to solve the high transportation cost caused by the low volume and energy density of biomass in large-scale industrial applications.[20] Thus, this processing method must not be rejected.

Molten salts can be utilized as an excellent heat storage and reaction medium due to high heat capacity and abundant catalytic ions,[21] and the use of molten NaOH for fast pyrolysis can be an effective way to solve the problems faced by ATT. The homogeneity of the liquid and fast heating rate significantly promotes the reaction between biomass/volatiles and NaOH. To the best of our knowledge, the fast pyrolysis properties within molten NaOH have only been explored in 2012 by Jiang et al.[22] They found that, as the temperature increased from 350 to 550 °C, the hydrogen yield of rice stalk increased at a rather constant rate. However, the hydrogen production capacity of molten NaOH at higher temperatures has not yet been investigated. On the one hand, biomass pellets inherently require a higher pyrolysis temperature than biomass powders for better conversion into gas products.[23,24] In addition, higher temperatures also enable the use of a wider range in molten salt composition (shown in Figure S1), which can increase molten salt utilization and improve operational safety (blockage caused by salt solidification). On the other hand, the application of molten salts extends the possibilities of integrating the ATT process with concentrated solar energy. Consequently, when the reaction enthalpy is provided by solar energy, the resulting solar ATT process is sustainable.[25,26]

In this paper, the hydrogen production capacity of *Nannochloropsis* sp. pellets fast pyrolysis in molten NaOH−Na_2CO_3 (AMSP, alkaline molten salt pyrolysis) is investigated at 550, 650, and 750 °C. NaOH−Na_2CO_3 with a mass ratio of 8:2 was chosen instead of pure NaOH as the reaction medium, mainly to reduce the corrosion of the molten salt, to improve the economy of the process and to potentially recover more metals.[27] The pyrolysis process and evolution of molten NaOH−Na_2CO_3, the characteristics of continuous hydrogen production, as well as the sources of hydrogen are discussed for the first time, which can provide comprehensive guidance for its large-scale applications.

2. MATERIALS AND METHODS

2.1. Materials. *Nannochloropsis* sp. was purchased from Yantai Hairong Biology Technology Co.,Ltd., it was first sieved with a 30 mesh sieve and then oven dried at 105 °C for 20 h before use. The algae pellet (Φ 6 mm × 6.5 mm, 0.23 ± 0.005 g, ∼1.25 g/cm^3) was prepared by granulating the dried algae powder in a cylindrical mold. The ultimate analysis and proximate analysis are listed in Table 1. More information of the algae composition can be found in our previous studies.[19]

Table 1. Ultimate Analysis and Proximate Analysis of Algae

ultimate analysis (wt %, d)					proximate analysis (wt %, d)		
C	H	N	S	O*	volatile	fix carbon	ash
45.76	6.43	7.67	0.74	33.95	82.45	12.10	5.45

d, dry basis. *, by difference.

Sodium carbonate and sodium hydroxide (powder, analytical purity >99.5%), and other reagents were all purchased from the Sinopharm Chemical Reagent Co., Ltd (Shanghai, China). A total of 110 g of sodium hydroxide and sodium carbonate were mechanically mixed in a mass ratio of 8:2 for subsequent formation of eutectic salts.

2.2. Experimental Methods. The experimental facility for pyrolysis in molten salt is shown in Figure S2. A 41 mm diameter by 250 mm long cylindrical graphite crucible (carbon content > 99.9) was used for AMSP experiments and was positioned vertically within an enclosure made of Hastelloy C276. The reactor enclosure was sealed by a flange, on which the feed tube (10 mm i.d. Hastelloy C 276) and bubble tube (1.7 mm i.d. Hastelloy C276) were arranged and sealed by graphite gaskets. Algae pellets were stored in the feeding unit and fed sequentially from the feed tube into molten salt. A flow of N_2 was introduced into the feed tube to create a positive pressure ensuring that the pellets were quickly immersed into the molten salt rather than floating. The height of salt in molten state in the crucible was about 45 mm (∼1.85 g/cm^3). A perforated plate (pore size of 1.2 mm) was arranged 8−10 mm beneath the molten salt surface to prevent the floating of particles. The openings for the feed tube and bubble tube were located 15 and 8 mm, respectively, above the bottom of the crucible.

For each AMSP experiment, approximately 2.3 g of algae pellets were loaded in advance in the feeding unit, a higher molten salt to feedstock mass ratio (around 50) was used for full immersion of algae pellets, even during continuous operation. In the future, the design of industrial reactors will undoubtedly be dominated by the continuous feed mode. As the continuous reaction proceeds, the ratio of molten salt to feedstock will decrease, and this process will be economically favorable. N_2 (250 mL/min) was introduced into the feed tube for 30 min to ensure an oxygen-free condition in the vessel. When the temperature rose to 400 °C, another N_2 (200 mL/min) was introduced into the bubbling tube to stir the molten salt for uniformly mixed and fully melting during the melting process of salt. After the temperature reached the targeted temperature (550, 650, and 750 °C), the algae pellets were fed into the molten salt, and the pyrolysis started.

The AMSP reaction can be described by reaction 2, the molecular formula of algae ($C_1H_{1.69}O_{0.56}N_{0.14}S_{0.006}$) is given based on the results of ultimate analysis listed in Table 1. Each AMSP experiment lasted for 20 min to achieve a large conversion rate of algae pellets in a shorter period of time, as some of the fine char particles will float on the surface of salt and greatly prolong the reaction time. The condensable volatiles captured in the ice-water bath (aluminum ball for enhancing heat transfer) were identified as a liquid containing bio-oil and water. Its yield was obtained by the weight difference. The non-condensable volatiles were filtered and collected by sample bags for GC (gas chromatography) analysis. The mixture in crucible (mainly salts and char) was dissolved with deionized water and then filtered to obtain a solid product (referred as char).

$$C_1H_{1.69}O_{0.56}N_{0.14}S_{0.006} + a\text{NaOH} \rightarrow b\text{Na}_2\text{CO}_3 + c\text{H}_2 + \text{salt} + \text{char} + \text{liquid} + \text{gas} \quad (2)$$

To compare with the AMSP reaction, standard pyrolysis and ATT experiments were also performed. For standard pyrolysis, the experimental procedures were exactly the same as that of the AMSP reaction, except that molten salt was not added. For the ATT reaction, the algae and molten salt were mixed in advance and then placed in the crucible for the reaction. The heating procedure was as follows: the temperature rose from room temperature to 110 °C in 20 min and maintained at 110 °C for 30 min and then rose to 750 °C at a heating rate of 4 °C/min and stayed at 750 °C for 20 min. After the reaction, the whole system was cooled to room temperature by carrier gas.

Each experiment was performed for 3−5 times to check the reproducibility of the experiments, and all the results in this paper were calculated based on ash-free dry basis. In addition, it is recommended to use Inconel series ($Ni_{72}Cr_{14}Fe_6Co_XTi_Y$) and Hastelloy C 276 ($Ni_{63.5}Cr_{14.5}Mo_{15}Fe_4W_3$) as the reactor materials to resist the corrosion of molten NaOH−Na_2CO_3 in practical industrial applications.[28,29]

2.3. Characterization. The gas products collected by sample bag were analyzed by a gas chromatography (Panna A91, Changzhou panna instrument Co., Ltd, China) equipped with a 5A molecular sieve column, a Porapak Q column, and an Al_2O_3/KCl capillary column. The real-time gas volume concentration was measured with an online gas analyzer (Gasboard-3100, Sifang photoelectric technologies Co., Ltd, China) with a test resolution of 0.01%. Details on the test methods and results processing of gas chromatography and online gas analyzer can be found in our previous work.[21,23] In addition, the real-time release characteristics of N/S/Cl^- containing gases were detected by an on-line portable Fourier infrared gas analyzer (Gasmet DX4000, Finland) with a scanning speed of 10 times/s and a mid-infrared full spectrum range from 900 to 4200 cm^{-1}. The analysis accuracy was ±3%of the corresponding calibration range.

The thermal stability and melting point of the molten salt were tested with an integrated thermal analyzer with thermogravimetric-differential calorimetry sensor (TGA/DSC -1,Mettler Toledo, Switzerland). More than 15 mg of salt was placed in a pure nickel crucible and its weight loss and endothermic property were recorded in the temperature range of 30−850 °C under a heating rate of 10 °C/min. The detailed composition of molten salt was measured by X-ray photoelectron spectroscopy (XPS, Thermo Fisher Scientific K-Alpha, America), field emission scanning electron microscopy (FE-SEM, Nova NanoSEM 450, Holland), and an X-ray diffraction (XRD) instrument (Bruker D8 Endeavor, United States of America). In addition, the content of NaOH and Na_2CO_3 in molten salts was measured five times according to ISO 3196:1975 (sodium hydroxide for industrial use-determination of carbonates content-titrimetric method) to obtain the average value.

3. RESULTS AND DISCUSSION

3.1. Pyrolysis Product Distribution. The effect of molten NaOH−Na_2CO_3 on the pyrolysis products distribution at different temperatures is presented in Figure 1. The

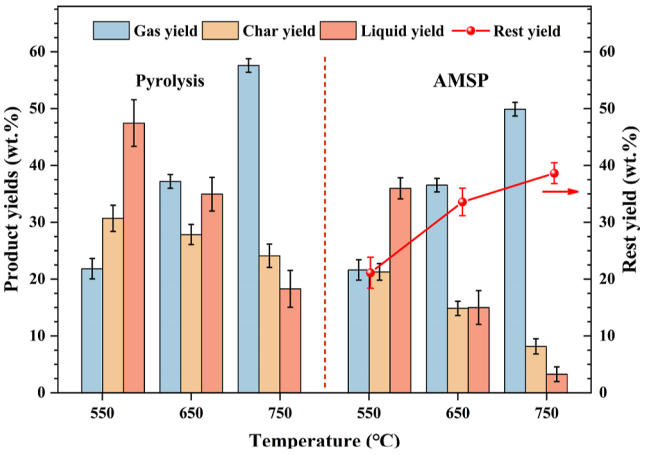

Figure 1. Product distribution as a function of temperature for standard pyrolysis and AMSP.

variation trend of pyrolysis products' yield with temperature in molten NaOH−Na_2CO_3 is similar to that of standard pyrolysis. The gas yield increases with temperature, while the liquid and char yields decrease, reaching 49.91, 3.28, and 8.17 wt %, respectively, at 750 °C. Except for the gas, liquid and char products, the rest of the feedstock is transferred to the molten salt (defined as the rest yield, which is obtained by difference), and its specific formation path and post-processing method are described in detail in Sections 3.5 and 3.6. However, the yields of gas, liquid, and char obtained by AMSP all decrease, especially at high temperatures. CO and CO_2 (CO_X) react with NaOH through reactions 3−4 resulting in a reduced gas yield, and the catalytic effect of molten salt enhances the secondary cracking of volatiles, leading to the reduction of liquid yield.[21,30] In addition, molten salt infiltrates the char pores and increases the exposed area of char (as shown in Figure S3), thus enhancing the reaction between char and molten salt, as shown in reactions 4−5.[31−33]

$$2\text{NaOH}_{(l)} + \text{CO}_{(g)} \rightarrow \text{Na}_2\text{CO}_{3(l)} + \text{H}_{2(g)} \quad (3)$$

$$4\text{NaOH}_{(l)} + \text{C}_{(s)} + \text{CO}_{2(g)} \rightarrow 2\text{Na}_2\text{CO}_{3(l)} + 2\text{H}_{2(g)} \quad (4)$$

$$\text{C}_{(s)} + \text{Na}_2\text{CO}_{3(l)} \rightarrow \text{Na}_2\text{O}_{(s)} + 2\text{CO}_{(g)} \quad (5)$$

3.2. Gas Product Composition. Figure 2 shows the composition of gas products for different pyrolysis media versus temperature. It should be noted that the gas yield based on per weight of algae does not imply that the gas is derived entirely from algae, which may also include a fraction supplied

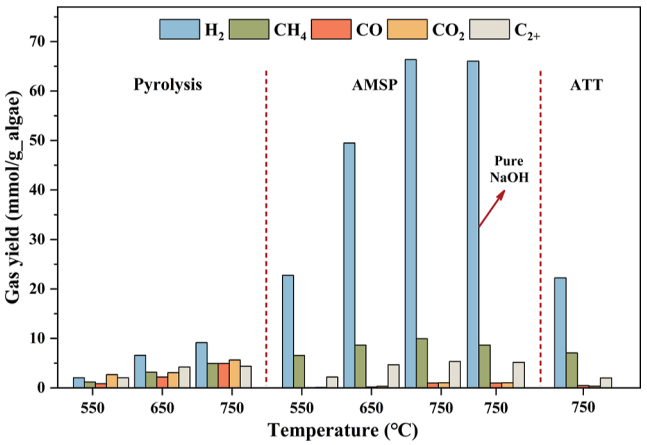

Figure 2. Gas product composition as a function of temperature for standard pyrolysis, AMSP, and ATT (C_{2+} contains C_2H_6, C_2H_4, C_2H_2, C_3H_8, C_3H_6, C_4H_{10}, C_4H_8, and C_5H_{10}).

by molten salt, and on this basis, we can compare the hydrogen yield of different processes. High temperatures promote the production of all gas components in the absence of molten salt, which is consistent with the existing studies.[34] Molten NaOH−Na_2CO_3 drastically increases the H_2 yield, suppresses CO_x production, and promotes the production of small amounts of CH_4 and C_{2+}.

At 750 °C, CO_x reacts with molten NaOH through reactions 3−4, leading to a high H_2 yield of 66.37 mmol/g-algae, which is 7 times higher than that of standard pyrolysis. In this condition, H_2, CH_4, and C_{2+} account for 79.98, 12.13, and 6.44 vol % of the gas product respectively. CH_4 mainly comes from the volatile fraction released by algae pyrolysis, as shown in reaction 6.[35] Compared to standard pyrolysis, AMSP and ATT have higher CH_4 yields due to the consumption of CO_2 and H_2O by molten salts, which inhibits the reforming of CH_4, as shown in reactions 7−8. The rest gas is 0.76 vol %CO_2 and 0.69 vol % CO,which is mainly due to the incomplete reaction of CO_x with molten salt caused by the extremely fast pyrolysis rate at high temperatures.

$$\text{Biomass} \xrightarrow{\text{pyrolysis}} [(C_xH_yO_z)_{tar} + (H_2 + CO + CO_2 + CH_4 + C_{2+})_{gas}]_{volatile} + (C + \text{ash})_{char} \quad (6)$$

$$CH_4 + CO_2 \rightarrow 2CO + 2H_2 \quad (7)$$

$$CH_4 + H_2O \rightarrow CO + 3H_2 \quad (8)$$

Additionally, it is worth mentioning that a series of ex situ catalysts such as modified nickel alloys (Ni−Co/Al_2O_3, Ni−Fe/zeolite, Ni/ZrO_2, etc.) were developed for the reforming of CH_4 and C_nH_m (including tar) to form hydrogen. Excellent results have been obtained,[14,36,37] which can be used as a post-treatment method to further improve the yield and purity of hydrogen.

The AMSP and ATT reactions in pure NaOH were also performed to compare the hydrogen production capacity, aiming to confirm whether the AMSP has an advantage over the ATT reaction and whether there is a difference between NaOH−Na_2CO_3 and pure NaOH. Molten NaOH yields about 3 times the amount of H_2 (66.05mmol/g-algae) compared to ATT (22.24 mmol/g-algae), suggesting a better performance of AMSP in hydrogen production. The yield of each gas (especially H_2) in molten NaOH and molten NaOH−Na_2CO_3 is basically the same, and there is little difference between these two salts. The main reason is that the molar amount of NaOH is in excess compared to that of algae and Na_2CO_3, which greatly weakens the contribution of Na_2CO_3 to the gas production.

3.3. Process of Algae AMSP. The gas release rate of algae pyrolysis with and without molten salt is calculated based on the real-time volume concentration of gas, where Figure 3 displays the results. Figure 3a shows that the pellet

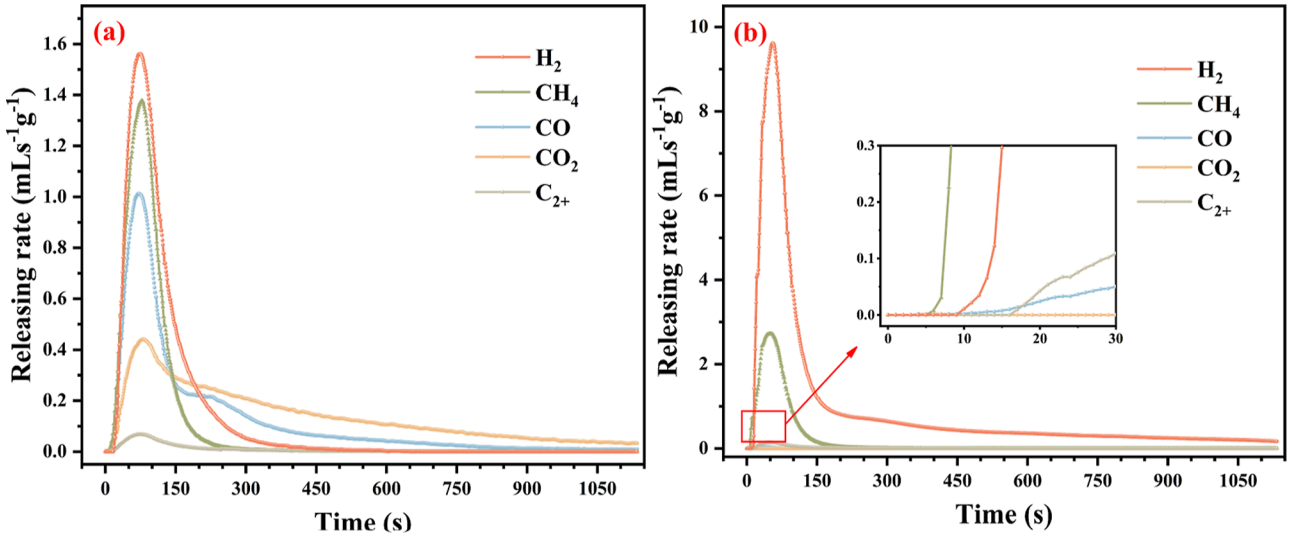

Figure 3. Gas release rate of algae pyrolysis at 750 °C (a) without molten salt and (b) with molten salt (C_{2+} contains C_2H_6, C_3H_8, C_4H_{10}, and C_5H_{12}).

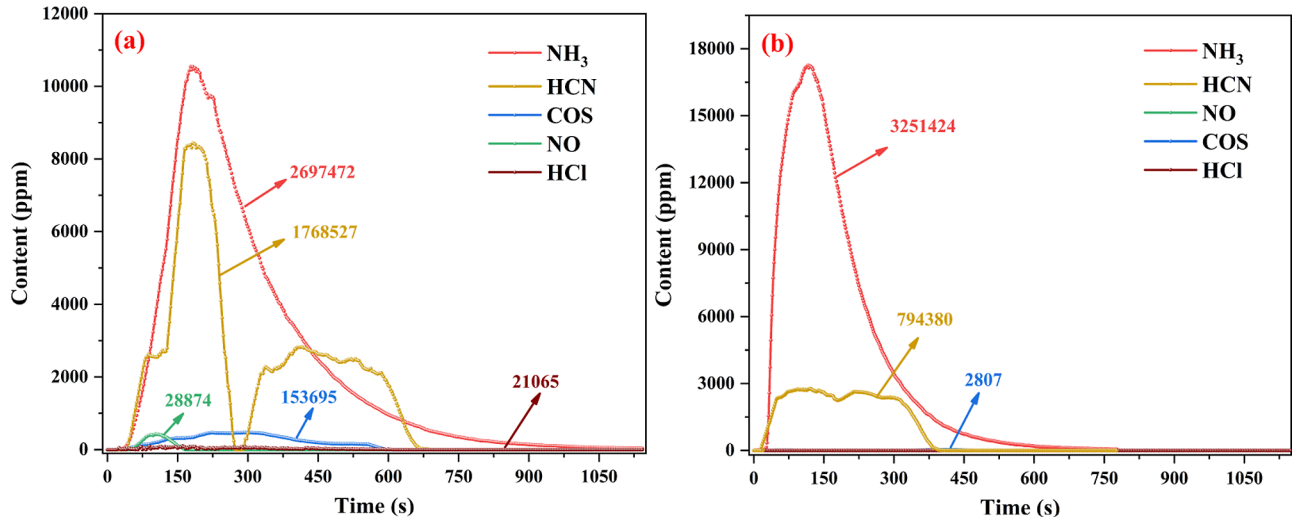

Figure 4. Pollution gas release rate of algae pyrolysis (a) without molten salt and (b) with molten salt.

pyrolysis without molten salt lasts for a long time due to the inferior heat and mass transfer. The maximum gas release rate occurs in the range of 71−81 s. Molten salt significantly increases the reaction rate and shortens the reaction time due to its efficient heat transfer and catalytic performance,[23] as shown in Figure 3b. Taking CH_4 as an example, the maximum release rate is approximately twice (from 1.38 to 2.72 mL s^{-1} g^{-1}) with the occurrence time decreasing by 34.2% (from 79 to 52 s). In addition, the increase of H_2 release rate (over 6 times) is the most significant (from 1.56 to 9.61 mL s^{-1} g^{-1}), while the release rates of CO and CO_2 are severely weakened. This is consistent with the gas yield results shown in Figure 2, mainly due to reactions 3−4. In addition, the H_2 peak appears later than the CH_4 peak in molten salt, which is contrary to standard pyrolysis, confirming the fact that other gas products are converted into H_2.

Figure 4 shows the pollution gas (mainly N/S/Cl containing gas) release characteristics of algae pyrolysis with and without molten salt, as these gases determine the application of the H_2-rich gas, along with its pre-treatment method. The areas under the curves, which are proportional to the total gas yield, are calculated by the integration of these evolution rates. The main pollution gas components of standard pyrolysis are NH_3 and HCN due to the high nitrogen content of algae. The release curve of HCN presents a double peak, which mainly originates from the decomposition of nitriles and pyridine-N in char, respectively.[34] The unexpected production of a small amount of NO under inert/reducing environment may be due to the decomposition of nitrates/nitrites and organic matter containing oxygen.[38]

In the presence of molten salt, the pollution gases are mainly composed of NH_3 and HCN in a mole ratio of roughly 4:1. The amount (about 1.2 times that of standard pyrolysis) and release rate of NH_3 increase due to the synergistic effect of high heating rate and abundant Na^+ provided by the molten salt. High heating rates accelerate the volatiles evolution and secondary reaction such as tar cracking, while Na^+ was reported to promote the generation of NH_3 by enhancing the reaction of amino acid pyrolysis.[21,39,40] The amount of HCN decreases by about 44.92% and COS/HCl/NO almost completely disappear, which is most likely due to the reactions with molten NaOH−Na_2CO_3 (shown in reactions 9−12) and the reducing atmosphere (higher H_2 content, reaction 13) during pyrolysis. The trapping effects of molten NaOH−Na_2CO_3 on these gases is supported by the elemental maps, as shown in Figure S4. Moreover, the XPS data in Figure S5 show that the chlorine, sulfur, and nitrogen elements in the molten salt are present in the form of Cl^-, S^{2-}, and CN^-, suggesting the conversion paths of HCN, COS, and HCl in molten NaOH−Na_2CO_3 given above are reasonable. It should be noted that the molten salt after five successive reactions (mentioned in the next section) was selected as the test sample due to the low content of Cl/S in algae.

$$NaOH_{(l)} + HCN_{(g)} \rightarrow NaCN_{(l)} + H_2O_{(g)}$$
$$\Delta G_{1023K} = -14.31\ \text{kJ} \quad (9)$$

$$Na_2CO_{3(l)} + HCN_{(g)} \rightarrow 2NaCN_{(l)} + H_2O_{(g)} + CO_{2(g)}$$
$$\Delta G_{1023K} = -9.15\ \text{kJ} \quad (10)$$

$$4NaOH_{(l)} + COS_{(g)} \rightarrow Na_2CO_{3(s)} + Na_2S_{(s)} + 2H_{2(g)}$$
$$\Delta G_{1023K} = -201.68\ \text{kJ} \quad (11)$$

$$NaOH_{(l)} + HCl_{(g)} \rightarrow NaCl_{(s)} + H_2O_{(g)} \quad (12)$$

$$2NO_{(g)} + 2H_{2(g)} \rightarrow N_{2(g)} + 2H_2O_{(g)}$$
$$\Delta G_{1023K} = -537.93\text{kJ} \quad (13)$$

In summary, molten NaOH−Na_2CO_3 exhibits very efficient S and Cl fixation properties, but is less effective in capturing N-containing gases, especially NH_3. Fortunately, oxygen carrier or iron-based/calcium-based additives were proved to be effective in inhibiting the formation of these NOx precursors by catalyzing/oxidizing them to harmless N_2 in situ.[41,42] Besides, some researchers have proved synergistic effects by coupling in situ catalysis (e.g., Ni/Al_2O_3, Ni−Fe/Al_2O_3, CeO_2, and so forth) in the fast pyrolysis process of molten salts.[43−45] Therefore, coupling oxygen carrier or iron-based/calcium-based catalysts in molten NaOH−Na_2CO_3 to reduce or remove these NOx precursors is a promising route.

3.4. Characteristics of Continuous Hydrogen Production.

A continuous and efficient operating system is essential for industrial applications; therefore, continuous

pyrolysis (five successive reactions) has been carried out to test the hydrogen production capacity of molten salt. Results are shown in Figure 5. As the reaction continues, the H_2 yield

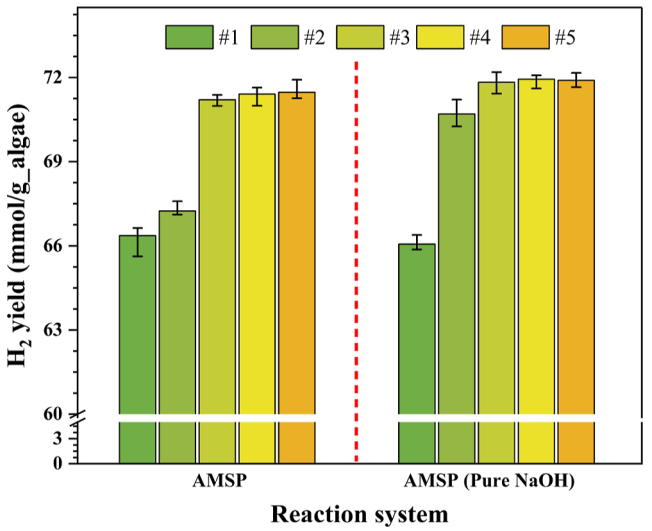

Figure 5. H_2 production during continuous pyrolysis in the two molten salts.

in molten NaOH−Na_2CO_3 rises during the first three reactions and then remained approximately stable, with an overall increase in H_2 yield from 66.37 mmol/g-algae to 71.48 mmol/g-algae. The increase in H_2 yield during the continuous reaction is due to that the residual char from the previous cycle reactions reacts with molten salt and releases H_2, as shown in reactions 4−5. Theoretically, even if the residual char floats on the surface of molten salt resulting in poor contact, it can still be completely converted if the reaction time is long enough.

The variation trend of H_2 yield and the final stable H_2 yield during the continuous pyrolysis in molten NaOH remain essentially the same as in molten NaOH−Na_2CO_3. This indicates that the proportion of NaOH to Na_2CO_3, within the tested range, does not affect the hydrogen production capacity during the continuous pyrolysis. On the other hand, molten salt can react with both algae and ash compounds during pyrolysis, which will in turn change its physicochemical properties and affects the algae conversion.[46,47] However, the maximum ash accumulation after five cycle reactions of algae will not exceed 0.6 wt % of the molten salt, the effect of ash on the hydrogen production capacity is negligible.[14] Previous studies have reported that ash occupies 20 wt % of the molten salt did not affect the reaction behavior based on the test results from a pilot scale molten salt coal gasifier during continuous operation.[13]

3.5. Evolution of Molten NaOH−Na_2CO_3. The evolution of molten salt during pyrolysis, especially con-tinuous pyrolysis, has rarely been studied, although it is important to guide practical industrial applications, such as the selection of reaction temperature, the setting of continuous pyrolysis duration and the regeneration of molten salts. Figure S6 shows the composition of molten salt after five cycle reactions, mainly consisting of NaOH, NaOH·H_2O (water absorption), and Na_2CO_3. Therefore, the proportion of NaOH and Na_2CO_3 can be represented by the content of OH^- and CO_3^{2-}. The detail content of NaOH and Na_2CO_3 in molten salt at different temperatures and during continuous pyrolysis process is presented in Figure 6. For a single test,

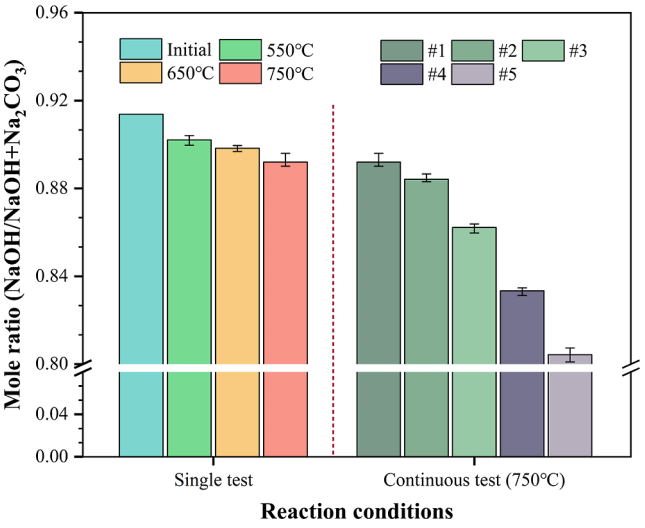

Figure 6. Variation of molten salt composition under different reaction conditions.

more NaOH is converted to Na_2CO_3 at high temperatures due to the high CO_X yield in pyrolysis gas, and the molar ratio of NaOH/(NaOH + Na_2CO_3) decreases from 0.914 to 0.892 as the temperature rises to 750 °C. For the continuous test, the molar ratio of NaOH/(NaOH + Na_2CO_3) decreased continuously and reached 0.804 after five successive reactions.

The hydrogen source and the hydrogen production efficiency are briefly calculated. Since 0.442 mol of NaOH is consumed after five successive reactions, a maximum of 0.442 mol of hydrogen can be produced in theory, as shown in eq 1. The total hydrogen yield of the five successive reactions is 0.756 mol, so at least 0.314 moles of hydrogen is produced from the algae feedstock. In fact, 11.5 g of algae could provide a maximum of 0.37 mol of hydrogen, so for AMSP reaction of algae pellets, the minimum theoretical hydrogen production efficiency is 84.86%, and at least 41.53% of hydrogen comes from the algae, with the rest coming from the NaOH effect. In addition, algae are used not only as a source of hydrogen but also as a source of carbon and water (dehydration from thermal decomposition) to achieve the extraction of hydrogen from NaOH.

The thermal stability and endothermic characteristics of different molten salts are further analyzed, and the results are shown in Figure 7. For the original molten salt (before reaction), the TG curve presents two stages (50−200 °C and >730 °C)of weight loss, and the DSC curve shows four endothermic peaks, labeled as A, B, C, and D. The first stage is due to the evaporation of water (formed during the sample preparation process), corresponding to the A peak (external water) and B peak (bound water, refer to the XRD results in Figure S6). The second stage (refer to the D peak) is caused by the vaporization of molten salts and the decomposition of Na_2CO_3 (reaction 14).[48−50] The C peak corresponds to the melting of salt.

$$Na_2CO_{3(l)} \rightarrow Na_2O_{(s)} + CO_{2(g)} \quad (14)$$

Overall, the three samples exhibit similar TG and DSG curves, indicating that they have similar properties to a certain

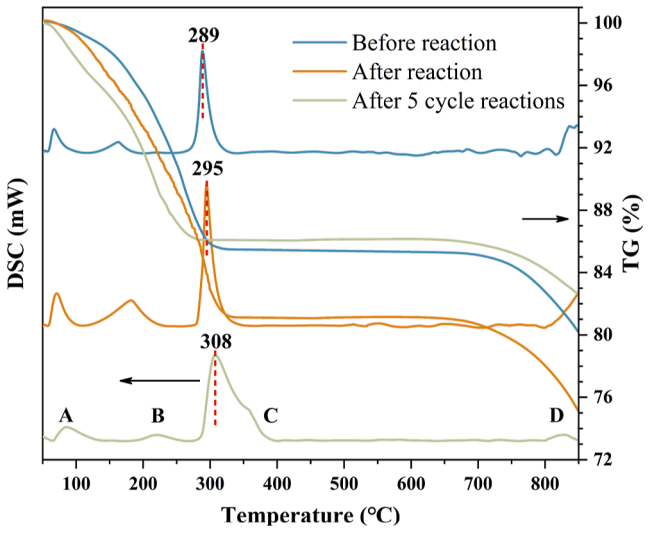

Figure 7. TG and DSC characteristics of molten salt before and after pyrolysis.

extent. The unsurprising increase in the melting point of molten salt after reaction is mainly due to the decrease in the mole ratio of NaOH/(NaOH + Na_2CO_3) (refer to Figure 6). The molten salt after five successive reactions has a smaller weight loss in the second stage compared to that of the other two samples. This may be caused by the inhomogeneity of the reacted molten salt (less Na_2CO_3 fraction), or by the accumulation of impurities such as NaCl, which has been proved to improve the thermal stability of molten salt at higher temperatures.[51] Preventing the solidification of molten salt at lower pyrolysis temperatures due to the increased melting point is essential to ensure safe operation, while higher thermal stability determines the efficiency of molten salt utilization.

3.6. Potential Applications of AMSP. In the present study, algae pellets are converted into H_2-rich gas (71.48 mmol/g-algae) with less CO_X (compared to standard pyrolysis) by the AMSP. The gas products can be applied as a raw material for the production of commodity chemicals such as ammonia and methanol,[52] and could even be fed into a polymer electrolyte membrane fuel cell without purification, as the very low CO_X content would not cause catalyst deactivation.[53] In addition, the gas products require less pretreatment before downstream applications because only two polluting gases, NH_3 and HCN, are present.

The use of pellet feedstock can greatly alleviate the high transportation cost of biomass due to its small bulk density; meanwhile, molten salt can effectively solve the deposition and melting of ash in raw materials during traditional hydrothermal liquefaction and gasification. Molten NaOH–Na_2CO_3 is also well suited for the treatment of some special organic solid wastes with high Cl/S content, such as PVC, waste tires, and waste plastics,[54,55] due to the excellent trapping performance of Cl/S containing gases. The reacted molten salt could be easily regenerated by cheap and readily available calcium hydroxide (e.g., industrial waste carbide slag),[14] avoiding the environmental and economic problems in the industrial process of preparing NaOH by electrolysis of NaCl. Moreover, the vast majority of carbon in CO_X could be eventually stored in the form of $CaCO_3$, realizing the carbon negativity of the whole process.[14]

Since molten NaOH–Na_2CO_3 has a large heat capacity, it can be used as a thermal storage medium to help alleviate solar energy intermittency. The introduction of concentrated solar energy (as shown in Figure 8) into the AMSP can efficiently provide the heat required for pyrolysis, which can avoid the criticism of high energy consumption,[56] although the operation temperature of AMSP (750 °C) is already lower compared with that of standard gasification (800–1200 °C). In this way, the AMSP can be developed as a green and efficient hydrogen production technology.

Phase diagram of NaOH–Na_2CO_3 mixtures, experimental setup, morphology of algae and its pyrolysis char, FSEM image and elemental mappings of the molten salt, XPS spectra of the molten salt, and XRD pattern of the molten salt (PDF)

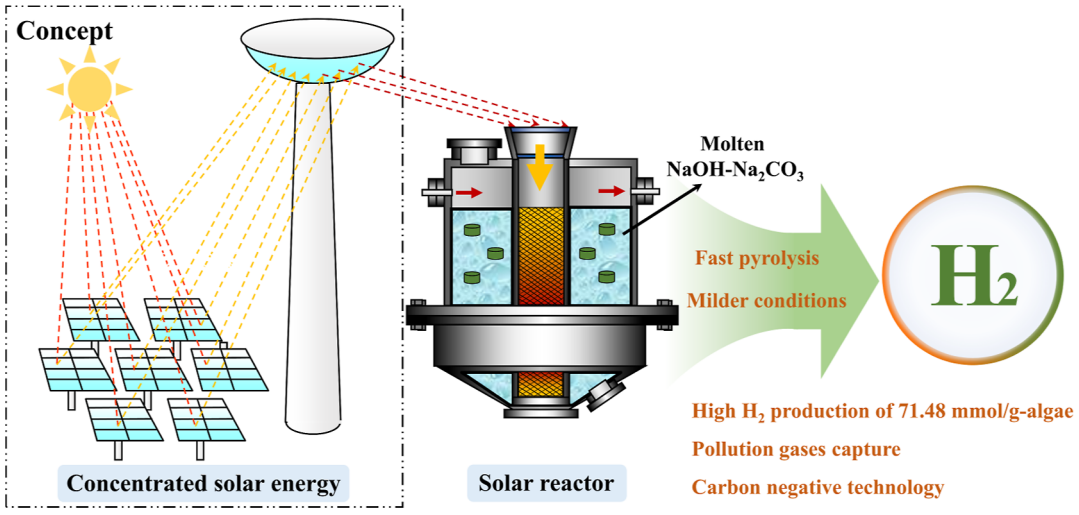

Figure 8. Concept of coupling concentrated solar energy with AMSP for hydrogen production.

AUTHOR INFORMATION

Corresponding Author

Kuo Zeng − *State Key Laboratory of Coal Combustion, Huaz hong University of Science and Technology, Wuhan, Hubei 430074, PR China;* orcid.org/0000-0001-8414-2636; Email: zengkuo666@hust.edu.cn

Authors

Jun Li − *State Key Laboratory of Coal Combustion, Huazhong University of Science and Technology, Wuhan, Hubei 430074, PR China*

Dian Zhong − *State Key Laboratory of Coal Combustion, Huazhong University of Science and Technology, Wuhan, Hubei 430074, PR China*

Gilles Flamant − *Processes, Materials and Solar Energy Laboratory, PROMES-CNRS, 66120 Odeillo Font Romeu, France*

Ange Nzihou − *Université de Toulouse, IMT Mines Albi, RAPSODEE CNRS UMR 5302, F.81013 Albi, France; Andlinger Center for Energy and the Environment, Princeton University, Princeton, New Jersey 08544, United States*

Claire E. White − *Andlinger Center for Energy and the Environment and Department of Civil and Environmental Engineering, Princeton University, Princeton, New Jersey 08544, United States*

Haiping Yang − *State Key Laboratory of Coal Combustion, Huazhong University of Science and Technology, Wuhan, Hubei 430074, PR China*

Hanping Chen − *State Key Laboratory of Coal Combustion, Huazhong University of Science and Technology, Wuhan, Hubei 430074, PR China*

Notes

The authors declare no competing financial interest.

ACKNOWLEDGMENTS

Authors acknowledge funding from the National Natural Science Foundation of China (52111530296 and 52261135626) and the support of National Natural Science Funds for Distinguished Young Scholar (52125601). In addition, authors would like to thank the Analytical and Testing Center in Huazhong University of Science & Technology (http://atc.hust.edu.cn) for the test.

REFERENCES

(1) Wang, W.; Cheng, B.; Zhao, M.; Anthony, E.; Luque, R.; Dionysiou, D. D. Boosting H_2 yield from photoreforming of lignocellulose by thermo-alkaline hydrolysis with selective generation of a key intermediate product: Tartaric acid. *Energy Convers. Manage.* **2022**, *257*, 115444.

(2) Wismann, S. T.; Engbæk, J. S.; Vendelbo, S. B.; Bendixen, F. B.; Eriksen, W. L.; Aasberg-Petersen, K.; Frandsen, C.; Chorkendorff, I.; Mortensen, P. M. Electrified methane reforming: A compact approach to greener industrial hydrogen production. *Science* **2019**, *364*, 756−759.

(3) Weng, Y.; Cai, W.; Wang, C. Evaluating the use of BECCS and afforestation under China's carbon-neutral target for 2060. *Appl. Energy* **2021**, *299*, 117263.

(4) Zabed, H. M.; Akter, S.; Yun, J.; Zhang, G.; Awad, F. N.; Qi, X.; Sahu, J. N. Recent advances in biological pretreatment of microalgae and lignocellulosic biomass for biofuel production. *Renewable Sustainable Energy Rev.* **2019**, *105*, 105−128.

(5) Jiang, H.; Wu, Y.; Fan, H.; Ji, J. Hydrogen Production from Biomass Pyrolysis in Molten Alkali. *AASRI Procedia* **2012**, *3*, 217−223.

(6) Deniz, I.; Vardar-Sukan, F.; Yüksel, M.; Saglam, M.; Ballice, L.; Yesil-Celiktas, O. Hydrogen production from marine biomass by hydrothermal gasification. *Energy Convers. Manage.* **2015**, *96*, 124−130.

(7) Farobie, O.; Matsumura, Y.; Syaftika, N.; Amrullah, A.; Hartulistiyoso, E.; Bayu, A.; Moheimani, N. R.; Karnjanakom, S.; Saefurahman, G. Recent advancement on hydrogen production from macroalgae via supercritical water gasification. *Bioresour. Technol. Rep.* **2021**, *16*, 100844.

(8) Bridgwater, A. V.; Peacocke, G. V. C. Fast pyrolysis processes for biomass. *Renewable Sustainable Energy Rev.* **2000**, *4*, 1−73.

(9) Saxena, S. K. Hydrogen production by chemically reacting species. *Int. J. Hydrogen Energy* **2003**, *28*, 49−53.

(10) Zhang, K.; Ouassil, N.; Campo, C. A. O.; Rim, G.; Kim, W.; Park, A. H. A. Kinetic and mechanistic investigation of catalytic alkaline thermal treatment of xylan producing high purity H2 with in-situ carbon capture. *J. Ind. Eng. Chem.* **2020**, *85*, 219−225.

(11) Stonor, M. R.; Ferguson, T. E.; Chen, J. G.; Park, A. H. A. Biomass conversion to H_2 with substantially suppressed CO_2 formation in the presence of Group I & Group II hydroxides and a Ni/ZrO_2 catalyst. *Energy Environ. Sci.* **2015**, *8*, 1702−1706.

(12) Zhao, M.; Cui, X.; Ji, G.; Zhou, H.; Vuppaladadiyam, A. K.; Zhao, X. Alkaline Thermal Treatment of Cellulosic Biomass for H_2 Production Using Ca-Based Bifunctional Materials. *ACS Sustain. Chem. Eng.* **2019**, *7*, 1202−1209.

(13) Trilling, C. A.; Martin, L. W. 500-MW combined-cycle power plant fueled with low-btu gas produced by the rockgas molten salt coal gasification process. 1979, *41*, 364-369.

(14) Zhang, K.; Kim, W.; Park, A. H. A. Alkaline thermal treatment of seaweed for high-purity hydrogen production with carbon capture and storage potential. *Nat. Commun.* **2020**, *11*, 3783.

(15) Zhou, H.; Park, A. H. A. Bio-energy with carbon capture and storage via alkaline thermal Treatment: Production of high purity H2 from wet wheat straw grass with CO_2 capture. *Appl. Energy* **2020**, *264*, 114675.

(16) Ishida, M.; Takenaka, S.; Yamanaka, I.; Otsuka, K. Production of CO_x-Free Hydrogen from Biomass and NaOH Mixture: Effect of Catalysts. *Energy Fuels* **2006**, *20*, 748−753.

(17) Wang, F.; Cheng, B.; Ting, Z. J.; Dong, W.; Zhou, H.; Anthony, E.; Zhao, M. Two-Stage Gasification of Sewage Sludge for Enhanced Hydrogen Production: Alkaline Pyrolysis Coupled with Catalytic Reforming Using Waste-Supported Ni Catalysts. *ACS Sustain. Chem. Eng.* **2020**, *8*, 13377−13386.

(18) Wu, X.; Wu, Y.; Wu, K.; Chen, Y.; Hu, H.; Yang, M. Study on pyrolytic kinetics and behavior: The co-pyrolysis of microalgae and polypropylene. *Bioresour. Technol.* **2015**, *192*, 522−528.

(19) Li, J.; Xiong, Z.; Zeng, K.; Zhong, D.; Zhang, X.; Chen, W.; Nzihou, A.; Flamant, G.; Yang, H.; Chen, H. Characteristics and Evolution of Nitrogen in the Heavy Components of Algae Pyrolysis Bio-Oil. *Environ. Sci. Technol.* **2021**, *55*, 6373−6385.

(20) Hu, Q.; Cheng, W.; Mao, Q.; Hu, J.; Yang, H.; Chen, H. Study on the physicochemical structure and gasification reactivity of chars from pyrolysis of biomass pellets under different heating rates. *Fuel* **2022**, *314*, 122789.

(21) Zeng, K.; Li, J.; Xie, Y.; Yang, H.; Yang, X.; Zhong, D.; Zhen, W.; Flamant, G.; Chen, H. Molten salt pyrolysis of biomass: The mechanism of volatile reforming and pyrolysis. *Energy* **2020**, *213*, 118801.

(22) Jiang, H.; Wu, Y.; Fan, H.; Ji, J. Hydrogen Production from Biomass Pyrolysis in Molten Alkali. *AASRI Procedia* **2012**, *3*, 217−223.

(23) Li, J.; Xie, Y.; Zeng, K.; Flamant, G.; Yang, H.; Yang, X.; Zhong, D.; Du, Z.; Chen, H. Biomass gasification in molten salt for syngas production. *Energy* **2020**, *210*, 118563.

(24) Zhang, S.; Yoshikawa, K.; Nakagome, H.; Kamo, T. Kinetics of the steam gasification of a phenolic circuit board in the presence of carbonates. *Appl. Energy* **2013**, *101*, 815−821.
(25) Yin, H.; Lu, B.; Xu, Y.; Tang, D.; Mao, X.; Xiao, W.; Wang, D.; Alshawabkeh, A. N. Harvesting Capacitive Carbon by Carbonization of Waste Biomass in Molten Salts. *Environ. Sci. Technol.* **2014**, *48*, 8101−8108.
(26) Xie, Y.; Zeng, K.; Flamant, G.; Yang, H.; Liu, N.; He, X.; Yang, X.; Nzihou, A.; Chen, H. Solar pyrolysis of cotton stalk in molten salt for bio-fuel production. *Energy* **2019**, *179*, 1124−1132.
(27) Liu, J.; Guo, X.; Liu, Y.; Jiang, X.; Huang, G. Effects of alkali-salt fusion process on recovery of amphoteric metals from waste printed circuit boards. *Miner. Process. Extr. Metall.* **2016**, *125*, 211−215.
(28) Xu, K.; Li, J.; Zeng, K.; Zhong, D.; Peng, J.; Qiu, Y.; Flamant, G.; Yang, H.; Chen, H. The characteristics and evolution of nitrogen in bio-oil from microalgae pyrolysis in molten salt. *Fuel* **2023**, *331*, 125903.
(29) Pooja, M.; Ravishankar, K. S.; Madav, V. High temperature corrosion behaviour of stainless steels and Inconel 625 in hydroxide salt. *Mater. Today: Proc.* **2021**, *46*, 2612−2615.
(30) Nzihou, A.; Stanmore, B.; Sharrock, P. A review of catalysts for the gasification of biomass char, with some reference to coal. *Energy* **2013**, *58*, 305−317.
(31) Nagase, K.; Shimodaira, T.; Itoh, M.; Zheng, Y. Kinetics and mechanisms of the reverse Boudouard reaction over metal carbonates in connection with the reactions of solid carbon with the metal carbonates. *Phys. Chem. Chem. Phys.* **1999**, *1*, 5659−5664.
(32) Nygård, H. S.; Danielsen, F.; Olsen, E. Thermal History of Wood Particles in Molten Salt Pyrolysis. *Energy Fuels* **2012**, *26*, 6419−6425.
(33) Ferguson, T. E.; Park, Y.; Petit, C.; Park, A. H. A. Novel Approach to Hydrogen Production with Suppressed CO_x Generation from a Model Biomass Feedstock. *Energy Fuels* **2012**, *26*, 4486−4496.
(34) Chen, W.; Yang, H.; Chen, Y.; Xia, M.; Chen, X.; Chen, H. Transformation of Nitrogen and Evolution of N-Containing Species during Algae Pyrolysis. *Environ. Sci. Technol.* **2017**, *51*, 6570−6579.
(35) Sikarwar, V. S.; Zhao, M.; Clough, P.; Yao, J.; Zhong, X.; Memon, M. Z.; Shah, N.; Anthony, E. J.; Fennell, P. S. An overview of advances in biomass gasification. *Energy Environ. Sci.* **2016**, *9*, 2939−2977.
(36) Wang, L.; Li, D.; Koike, M.; Watanabe, H.; Xu, Y.; Nakagawa, Y.; Tomishige, K. Catalytic performance and characterization of Ni−Co catalysts for the steam reforming of biomass tar to synthesis gas. *Fuel* **2013**, *112*, 654−661.
(37) Ahmed, T.; Xiu, S.; Wang, L.; Shahbazi, A. Investigation of Ni/Fe/Mg zeolite-supported catalysts in steam reforming of tar using simulated-toluene as model compound. *Fuel* **2018**, *211*, 566−571.
(38) Liu, H.; Zhang, Q.; Hu, H.; Liu, P.; Hu, X.; Li, A.; Yao, H. Catalytic role of conditioner CaO in nitrogen transformation during sewage sludge pyrolysis. *Proc. Combust. Inst.* **2015**, *35*, 2759−2766.
(39) Ma, M.; Bai, Y.; Wang, J.; Song, X.; Su, W.; Wang, F.; Yu, G. Thermal conversion behavior and nitrogen-containing gas products evolution during co-pyrolysis of cow manure and coal: A thermal gravimetric analyzer/differential scanning calorimetry−mass spectrometer investigation. *Asia-Pac. J. Chem. Eng.* **2021**, *16*, No. e2663.
(40) Chen, H.; Shan, R.; Zhao, F.; Gu, J.; Zhang, Y.; Yuan, H.; Chen, Y. A review on the NOx precursors release during biomass pyrolysis. *Chem. Eng. J.* **2023**, *451*, 138979.
(41) Yi, L.; Liu, H.; Lu, G.; Zhang, Q.; Wang, J.; Hu, H.; Yao, H. Effect of Mixed Fe/Ca Additives on Nitrogen Transformation during Protein and Amino Acid Pyrolysis. *Energy Fuels* **2017**, *31*, 9484−9490.
(42) Guo, S.; Liu, T.; Hui, J.; Che, D.; Li, X.; Sun, B.; Li, S. Effects of calcium oxide on nitrogen oxide precursor formation during sludge protein pyrolysis. *Energy* **2019**, *189*, 116217.
(43) Wei, Y.; Wang, H.; He, F.; Ao, X.; Zhang, C. CeO2 as the Oxygen Carrier for Partial Oxidation of Methane to Synthesis Gas in Molten Salts: Thermodynamic Analysis and Experimental Investigation. *J. Nat. Gas Chem.* **2007**, *16*, 6−11.
(44) Hu, X.; Hu, Y.; Xu, Q.; Wang, X.; Li, G.; Cheng, H.; Zou, X.; Lu, X. Molten salt-promoted Ni-Fe/Al_2O_3 catalyst for methane decomposition. *Int. J. Hydrogen Energy* **2020**, *45*, 4244−4253.
(45) Ratchahat, S.; Srifa, A.; Koo-amornpattana, W.; Sakdaronnarong, C.; Charinpanitkul, T.; Wu, K. C. W.; Show, P.; Kodama, S.; Tanthapanichakoon, W.; Sekiguchi, H. Syngas production with low tar content from cellulose pyrolysis in molten salt combined with Ni/Al_2O_3 catalyst. *J. Anal. Appl. Pyrolysis* **2021**, *158*, 105243.
(46) Shen, J.; Hu, H.; Xu, M.; Liu, H.; Xu, K.; Zhang, X.; Yao, H.; Naruse, I. Interactions between molten salts and ash components during Zhundong coal gasification in eutectic carbonates. *Fuel* **2017**, *207*, 365−372.
(47) Xu, S.; Hu, H.; Guo, G.; Gong, L.; Liu, H.; Yao, H. Investigation of properties change in the reacted molten salts after molten chlorides cyclic thermal treatment of toxic MSWI fly ash. *J. Hazard. Mater.* **2022**, *421*, 126536.
(48) Lehman, R. L.; Gentry, J. S.; Glumac, N. G. Thermal stability of potassium carbonate near its melting point. *Thermochim. Acta* **1998**, *316*, 1−9.
(49) Jalalabadi, T.; Moghtaderi, B.; Allen, J. Thermochemical Conversion of Biomass in the Presence of Molten Alkali-Metal Carbonates under Reducing Environments of N_2 and CO_2. *Energies* **2020**, *13*, 5395.
(50) Olivares, R.; Chen, C.; Wright, S. The Thermal Stability of Molten Lithium-Sodium-Potassium Carbonate and the Influence of Additives on the Melting Point. *J. Sol. Energy Eng.* **2012**, *134*, 134.
(51) Gimenez, P.; Fereres, S. Effect of Heating Rates and Composition on the Thermal Decomposition of Nitrate Based Molten Salts. *Energy Procedia* **2015**, *69*, 654−662.
(52) Si, X.; Zhao, Z.; Chen, J.; Lu, R.; Lu, F. Low-Temperature Efficient Hydrogen Production from Raw Biomass on the Ni-Mo Catalyst. *ACS Catal.* **2022**, *12*, 10629−10637.
(53) Ye, S. *PEM Fuel Cell Electrocatalysts and Catalyst Layers: Fundamentals and Applications*; Zhang, J., Eds.; Springer London: London, 2008; pp. 759-834.
(54) Ephraim, A.; Pozzobon, V.; Lebonnois, D.; Peregrina, C.; Sharrock, P.; Nzihou, A.; Pham Minh, D. Pyrolysis of wood and PVC mixtures: thermal behaviour and kinetic modelling. In *Biomass Conversion and Biorefinery*; Springer, 2020.
(55) Wang, H.; Hu, H.; Yang, Y.; Liu, H.; Tang, H.; Xu, S.; Li, A.; Yao, H. Effect of high heating rates on products distribution and sulfur transformation during the pyrolysis of waste tires. *Waste Manage.* **2020**, *118*, 9−17.
(56) Zhong, D.; Chang, Z.; Zeng, K.; Li, J.; Qiu, Y.; Lu, Q.; Flamant, G.; Yang, H.; Chen, H. Solar pyrolysis of biomass - part II: The physicochemical structure evolution of char. *Fuel* **2023**, *333*, 126474.